












RESEARCH ARTICLE | JUNE 24 2024

Tunable topological domain structures in high-density PbTiO₃ nanodots array

Hongying Chen; Zhiyu Liu; Guo Tian ; Gui Wang; Yihang Guo; Zongwen Duan; Di Wu ; Yu Deng ; Guoyu Wang ; Zhipeng Hou ; Deyang Chen ; Zhen Fan ; Minghui Qin ; Ji-Yan Dai ; Jun-Ming Liu ; Xingsen Gao 



Appl. Phys. Lett. 124, 262901 (2024)

<https://doi.org/10.1063/5.0213936>



Articles You May Be Interested In

Ferroelectric critical size and vortex domain structures of PbTiO₃ nanodots: A density functional theory study

J. Appl. Phys. (March 2018)

Domain evolution in BiFeO₃ epitaxial nanoisland array via post-annealing

J. Appl. Phys. (October 2024)

Abnormal topological domains in a high-density array of ferroelectric nanodots

J. Appl. Phys. (March 2023)

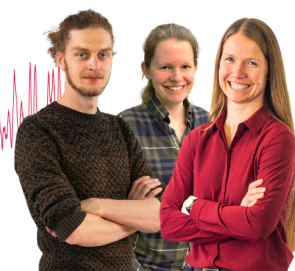
Webinar From Noise to Knowledge

May 13th – Register now



Zurich
Instruments

Universität
Konstanz



Tunable topological domain structures in high-density PbTiO₃ nanodots array

Cite as: Appl. Phys. Lett. **124**, 262901 (2024); doi: [10.1063/5.0213936](https://doi.org/10.1063/5.0213936)

Submitted: 14 April 2024 · Accepted: 2 June 2024 ·

Published Online: 24 June 2024



View Online



Export Citation



CrossMark

Hongying Chen,^{1,2} Zhiyu Liu,² Guo Tian,^{1,3,a)} Gui Wang,¹ Yihang Guo,¹ Zongwen Duan,¹ Di Wu,² Yu Deng,² Guoyu Wang,^{4,a)} Zhipeng Hou,¹ Deyang Chen,¹ Zhen Fan,¹ Minghui Qin,¹ Ji-Yan Dai,⁵ Jun-Ming Liu,^{1,5} and Xingsen Gao,^{1,a)}

AFFILIATIONS

¹Guangdong Provincial Key Laboratory of Quantum Engineering and Quantum Materials and Institute for Advanced Materials, South China Academy of Advanced Optoelectronics, South China Normal University, Guangzhou 510006, China

²National Laboratory of Solid-State Microstructures, Department of Materials Science and Engineering, and Jiangsu Key Laboratory of Artificial Functional Materials, Nanjing University, Nanjing 210093, China

³Department of Applied Physics, Hong Kong Polytechnic University, Hong Kong, China

⁴College of Materials Science and Engineering and Center of Quantum Materials and Devices, Chongqing University, Chongqing 401331, People's Republic of China

⁵Laboratory of Solid-State Microstructures and Innovation Center of Advanced Microstructures, Nanjing University, Nanjing 210093, China

^{a)}Authors to whom correspondence should be addressed: guotian@m.scnu.edu.cn; gywang2022@cqu.edu.cn; and xingsengao@scnu.edu.cn

ABSTRACT

In this work, we demonstrated that tunable topological domain structures, e.g., center-type domains and skyrmion-like polar bubbles, can be generated at room temperature in high-density epitaxial PbTiO₃ nanodots fabricated via the template-assisted tailoring of thin films. These topological domain structures can be manipulated electrically by applying an appropriate bias on the conductive atomic force microscopy tip, allowing for writing, erasing, and rewriting of topological domains into the nanodot. Moreover, ring-shaped conductive channels are observed around the center-type domain states. These findings provide a playground for further exploring their emerging functionalities and application potentials for nanoelectronics.

Published under an exclusive license by AIP Publishing. <https://doi.org/10.1063/5.0213936>

Exotic topological domain structures in ferroelectric materials, such as vortices,^{1–3} flux-closures,^{4–6} center domains,^{7–12} skyrmions,^{13–15} bubbles,^{16–21} and merons,²² have been extensively studied to comprehend their physical properties as well as potential for high-density memories,^{23–28} low-power consumption transistors,²⁹ and ferroelectric-based nanoelectronic devices.³⁰ These topological domains exhibit intriguing physical properties, including high stability attributable to topological protection, enhanced piezoelectric properties,³¹ enhanced conductive channels,^{32–34} and negative capacitance³⁵ among others. However, their functional and structural complexity present challenges in efficiently identifying and manipulating the topological states.

Theoretical studies propose that the formation of topological domains in ferroelectric materials can be attributed to a delicate equilibrium among elastic, electrostatic, and gradient energies.^{36,37} Substantial efforts have been made to produce and analyze topological

domains in recent years. For instance, it is reported that polar skyrmions can be stable in confined layers of PbTiO₃ (PTO) in PTO/SrTiO₃ (PTO/STO) superlattices.¹³ A group of topological center domains, including center-convergent domains, center-divergent domains, and double-center domains, has been discovered in small BiFeO₃ (BFO) nanodots with a lateral size of 60 nm.⁷ These center-type domains can be reversibly switched between convergent and divergent states, enabling the individual manipulation of the nanodots via electric fields. Ma *et al.*⁸ further discovered that the center-type quad-domain exhibits a remarkable ability to transition reversibly between a divergent state, characterized by highly conductive confined walls, and a convergent state, characterized by insulating confined walls. This finding highlights the immense potential of this quad-domain in storage applications, as it enables nondestructive readout of topological center-domain states. More recently, there have been

reports of high-density skyrmion-like polar nanodomains in freestanding PTO/STO bilayers that were transferred onto the Si substrate, which indicated the application potential in silicon-based nanodevices.¹⁴ However, creating and erasing these topological polar domains in precise dimensions at prescribed positions in a simple and controllable way, which is essential for on-demand designs and applications of these exotic domain structures, is still elusive.

It should also be noted that the center-type topological domains reported so far predominantly rely on rhombohedral phase ferroelectric films and nanostructures, for example, isolated BFO and Pb(Zr_{0.7}Ti_{0.3})O₃ (PZT) nanoislands tailored from thin films,^{7,9} self-assembled BFO nanoislands embedded in tetragonal BFO matrix,⁸ etc. This greatly restricts the selection of systems available for studying topological center domains. Previous research results suggested that dimension reduction down to nanoscale is an effective strategy to manipulate topological defects. In nanoscale confined systems, e.g., nanodots/nanoislands, the surface or edge effects and flexoelectric effect generated by the possible nonuniform strain can drive the polarization away from their original directions to form more complex domain textures.^{7,27,42,43} Therefore, it is intriguing to investigate whether these topological center-type states can maintain stability in structural systems apart from rhombohedral phase via the size effect. For this, we explore the domain structure in the PTO nanodots via tailoring of tetragonal films. Compared to the rhombohedra phase of BFO, PTO systems typically exhibit a-c domain states and have a much higher bandgap of around 3.4 eV, which may bring forth some different aspects in electronic and domain evolution properties.

In this work, we demonstrate the coexistence of different types of topological domain structures, e.g., center-type domains and skyrmion-like polar bubbles, in a high-density array of PTO nanodots fabricated via the template-assisted tailoring of tetragonal PTO thin films. These topological domain states can be electrically written, erased, and rewritten into the nanodot by utilizing an electrically biased atomic force microscopy (AFM) tip. Moreover, ring-shaped conductive channels have been observed surrounding these topological domains. The findings offer a valuable opportunity for in-depth exploration of their emerging functionalities and potential applications in nanoelectronics.

To begin, we start from the PTO nanodots array fabrication. The PTO thin films were first deposited on SrRuO₃ (SRO) buffered (100)-oriented SrTiO₃ (STO) substrates via pulsed laser deposition (PLD) using a KrF excimer laser (wavelength $\lambda = 248$ nm) at 680 °C in 15 Pa oxygen at a fluence of 55 mJ at 8 Hz. The microstructures and ferroelectric properties of the as grown PTO thin films are illustrated in Fig. S1. The PTO film is in a single c-domain state with the polarization completely in the out-of-plane direction. The ordered PTO nanodot arrays were patterned via a mask-assisted Ar⁺ beam etching method. Figure S2(a) shows the schematic diagram of the fabrication process. The etching details can be referred to our previous work.³⁸ In brief, a monolayer of polystyrene spheres (PS, with lateral size of 200 nm) was first transferred onto the as grown PTO epitaxial film to form an ordered and close-packed template. Then, the PS were etched to the desired size by oxygen plasma to form a discrete array. This was followed by an Ar⁺ ion beam etching process. Finally, the PS template was lifted off with chloroformic solution to obtain ordered PTO nanodot arrays.

We then examined the patterned sample from the PTO film, which exhibits a well-arranged array of nanodots with average lateral

size and height of 80 and 35 nm, as illustrated in the scanning electron microscopy (SEM) and atomic force microscopy (AFM) topographical images in Fig. 1(a) and Fig. S2(b), respectively. A rough estimation based on 80 nm lateral size of nanodots gives a high information memory density above 200 Gbit/in². The microstructures of the nanodots sample were then examined by cross-sectional transmission electron microscopy (TEM) image, as shown in Fig. 1(b). A clear isolated PTO nanodots array was observed in the mesa. The high-resolution TEM image of a selected area in Fig. 1(b) is shown in Fig. 1(c), demonstrating the high-quality epitaxial structure. The x-ray diffraction (XRD) θ -2 θ spectrum in Fig. 1(d) reveals the good epitaxy structure of the nanodots. This is evidenced by the presence of diffraction peaks originating from the substrate STO (002), bottom electrode SRO (002), and PTO (002). Moreover, the epitaxy structure is further confirmed by the (002) reciprocal space map (RSM) shown in Fig. 1(e). The out-of-plane lattice constant is 4.151 Å, close to that PTO thin films.

To see the domain structures, these nanodots were examined using vector piezoresponse force microscopy (PFM). This technique enables the mapping of both vertical and lateral amplitudes (L-amplitude and V-amplitude) as well as phases (L-phase and V-phase) of piezoresponse signals simultaneously. Figures 2(a) and 2(b) show topography and vertical PFM phase images of a selected PTO nanodots array. We can see in V-phase image in Fig. 2(b), some of the nanodots have single dark (bright) phase contrast, suggesting the favorable upward (downward) out-of-plane polarization component. The rest of the nanodots show double contrast, indicating the coexistence of upward and downward out-of-plane polarization in each nanodots. Figures 2(c) and 2(d) show the lateral PFM amplitude and phase images obtained when the cantilever was aligned at 0° and 90°, respectively, relative to the [010] direction. The corresponding PFM image captured at 45° is shown in Fig. S3. It was found that most of the nanodots have the half-dark and half-bright contrast in the lateral phase captured in both two cantilever rotation angles. These features are confirmed by the presence of a distinct, dark line in the lateral amplitude images, displaying a domain wall-like characteristics for the subsequent polarization component along the <010> direction. In addition, a small number of nanodots have single contrast.

As shown in Figs. 2(e) and 2(f), we chose two representative nanodots with magnified PFM images captured at 0°, 45°, and 90° sample rotation angles as paradigms. Based on both lateral phase and amplitude data, one can derive a 2D vector polarization distribution map using the MATLAB program following the method proposed by Kalinin *et al.*³⁹ The result indicates that the domain structures of these two types of PTO nanodots are center-convergent domain with downward polarization and center-divergent domain with upward polarization. These domain structures are somewhat similar to the center domains in small BFO nanodots (60 nm in diameter), where the polarizations rotate continuously. Based on these findings, we also presented a comprehensive three-dimensional polarization distribution of the center domain structures, as illustrated in Figs. 2(g) and 2(h).

Equally exciting is the discovery of skyrmion-like polar bubbles in some PTO nanodots, as illustrated in Fig. 3. Figure 3(a) shows the vertical PFM phase and amplitude images of a selected nanodots array. We can observe that the majority of the out-of-plane polarization components of the nanodots exhibit cylindrical bubble domain structures, as shown in Fig. 3(a). However, a clear ring-shaped domain wall feature is present in the corresponding location in the vertical amplitude image.

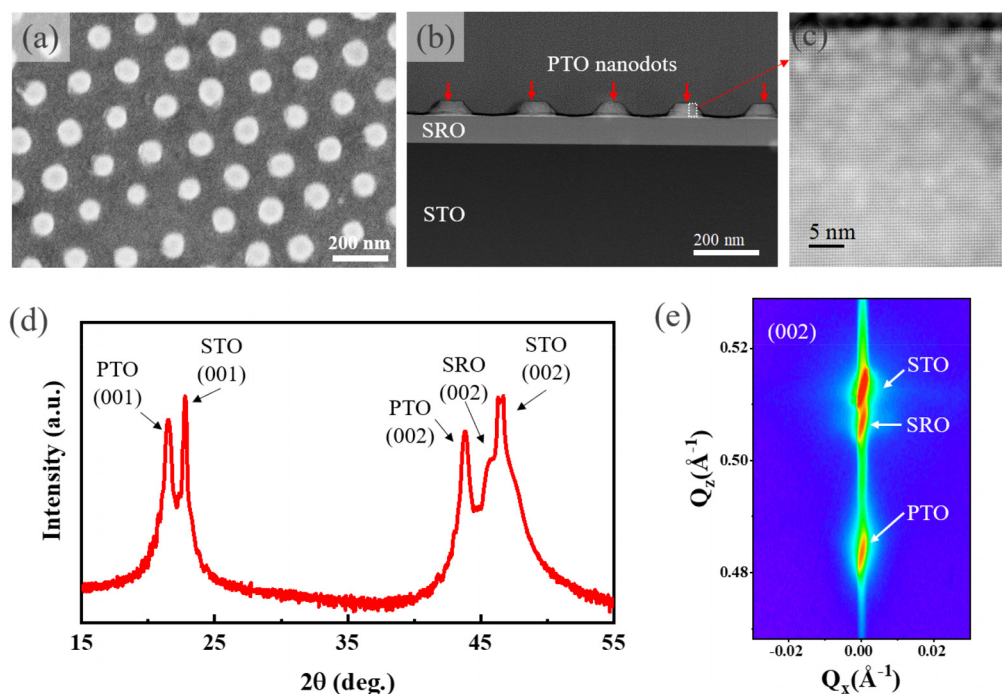


FIG. 1. (a) SEM image of a selected PTO nanodots array. (b) Cross-sectional SEM image of a PTO nanodots array. (c) High resolution TEM magnification image for the selected area in panel (b). The θ - 2θ scan diffraction pattern (d) and reciprocal space map (RSM) (e) measured at around (103) plane direction of the PTO nanodots array.

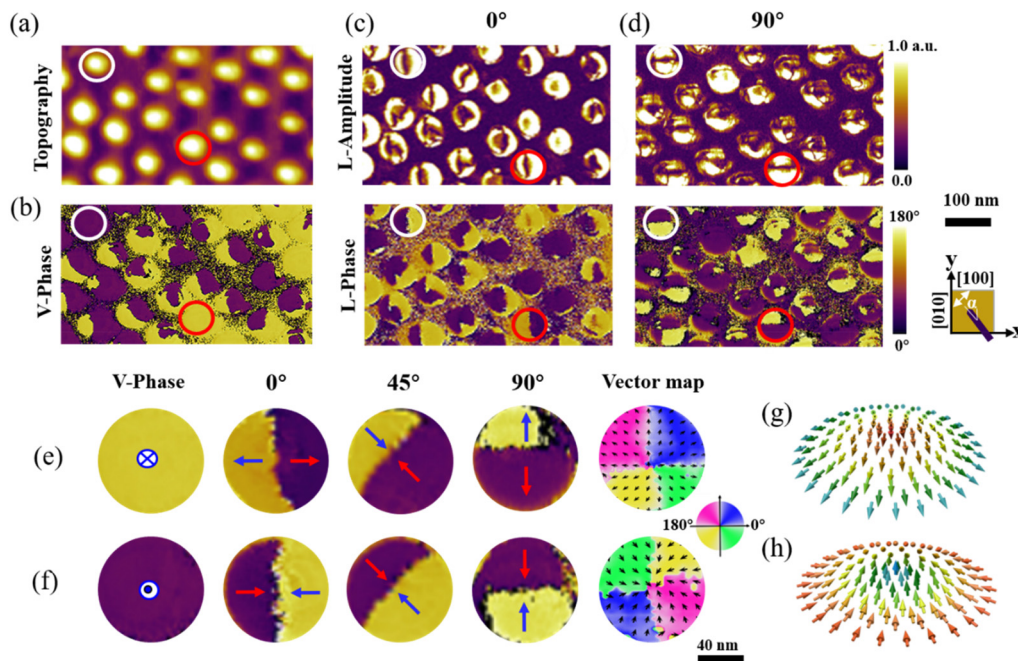


FIG. 2. (a) Topography image of the selected PTO nanodots array measured by AFM. (b) Vertical PFM phase image. (c) and (d) Lateral PFM amplitude and phase images obtained by aligning the cantilever at 0° and 90° to the [010] direction, as shown in the inset. (e) and (f) Magnified PFM images of the nanodots indicated by white circle and red circles in the corresponding images. (g) and (h) Schematic three-dimensional polarization distribution of the PTO nanodots.

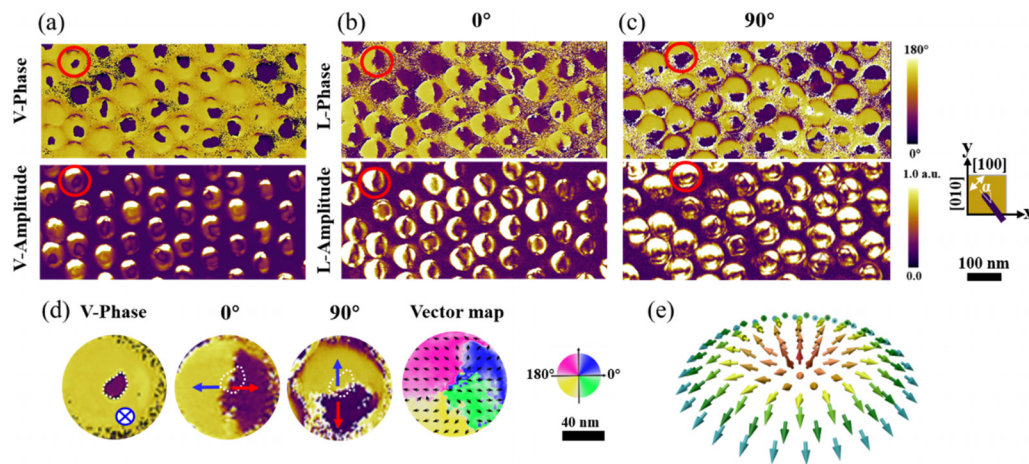


FIG. 3. (a) Vertical PFM amplitude and phase images of the PTO nanodots array. (b) and (c) Lateral PFM amplitude and phase images obtained by aligning the cantilever at 0° and 90° to the [010] direction, as shown in the inset. (d) Magnified PFM images of the nanodots indicated by red circles in the corresponding images. (e) Schematic three-dimensional polarization distribution of the PTO nanodots.

Figures S3(b) and S3(c) present the lateral PFM phase and amplitude images obtained when aligning the cantilever at 0°, 45°, and 90°, respectively, relative to the [010] direction. Clear dark lines are observed in the lateral amplitude images of the bubble domains. These lines separate the lateral phase images of the bubble domain into two halves, exhibiting a 180° phase contrast. It is worth noting that these lines are consistently aligned with the cantilever and rotate in accordance with its movement. This indicates that the bubble domains exhibit an in-plane polarization configuration that is antisymmetric, with rotational symmetry around the out-of-plane axis passing through the center of the domain. Combining the vertical and lateral PFM results, one may identify that these are divergent nanodomains, in which the upward polarization at the core gradually diverges away from the center and ultimately transitions to a downward orientation along the periphery of these nanodomains, as shown in the schematic polarization distribution in Fig. 3(d), similar to the spin configuration of a Néel-type skyrmion in ferromagnetics⁴⁰ as well as the reported results in freestanding STO/PTO bilayers transferred on Si substrates.¹⁴

The observation of these topological domains in PTO nanodots is intriguing, as it reveals a deviation in the polarization from the typically observed out-of-plane orientations in tetragonal phase PTO. The formation of these domains is probably driven by the competitions among depolarization energy, polarization-strain coupling, and surface strain, all of which can greatly change the local anisotropy and thus the polarization distribution. The similar center domains with continuous rotational polarization instead of the earlier reported quadrant center domains have been reported in BFO nanodots with lateral size of 60 nm in our previous work.⁷ Moreover, the potential existence of nonuniform strain in the nanodots can induce flexoelectric rotations, thereby causing the polarization to deviate from its original orientation. Figure S4 shows the reciprocal space mappings of PTO films and nanodots around (002) diffraction of STO substrate before and after etching, respectively. The out of plane reciprocal vector of the nanodots sample increases compared to the films, indicating the decrease in the out of plane lattice parameter. The nanodots were studied in atomic resolution by observing a cross section through high angle

annular dark field scanning transmission electron microscopy (HAADF-STEM) from the [010] zone axis in Fig. S5(a). The GPA ϵ_{xx} (in-plane) map in Fig. S5(b) shows the strain variations along the direction parallel to the interface, indicating the increase in the in-plane lattice parameter. This is because the nanodots etched from the thin film reduced the clamping effect from the substrate, resulting in a fast lattice strain relaxation in nanodots. These findings suggested that reducing the dimensions to the nanoscale is a viable approach to manipulate and control topological defects.

In addition, these topological domains in PTO nanodots can be reversibly switched. We next study the evolution of these topological domains by applying scanning bias at various voltages using conductive tip. As demonstrated in Fig. 4(a), the selected PTO nanodots show center-up skyrmion-like polar bubble structures. After scanning the tip biased at -2 V, the out-of-plane cylindrical bubble domains grow to form single domains, while the lateral PFM phases show uniform half-dark and half-bright contrast. Combining the vertical and lateral PFM signals, it can be discovered that the center-up skyrmion-like polar bubble domains switched to center convergent domains with upward polarization [Fig. 4(b)]. Then, by scanning the tip biased at 2.5 V, the center-up skyrmion-like polar bubbles appear again. PFM measurements in Fig. 4(c) show that both the vertical and the lateral PFM phases are reversed as compared to the domain states in the as-prepared sample, indicating that these nanodomains are center divergent with the center polarization pointing upward. As the positive bias increases to 3.5 V, the upward *c*-domains in the center of the nanodots are completely switched downward. The center-up skyrmion-like polar bubbles switched to center divergent with the central polarization pointing downward [Fig. 4(d)]. Finally, by scanning the tip biased at -2 V, the center divergent states switched to center convergent states again [Fig. 4(e)]. These topological domains can be switched multiple times, and both remain stable for over 48 h at room temperature, as shown in Fig. S6.

Conductive atomic force microscopy (CAFM) measurements are performed on the selected nanodots to study the transport characteristics of the center domains. The current map measured by a -1.5 V (+1.5 V bottom electrode bias in the CAFM mode) scan shows that

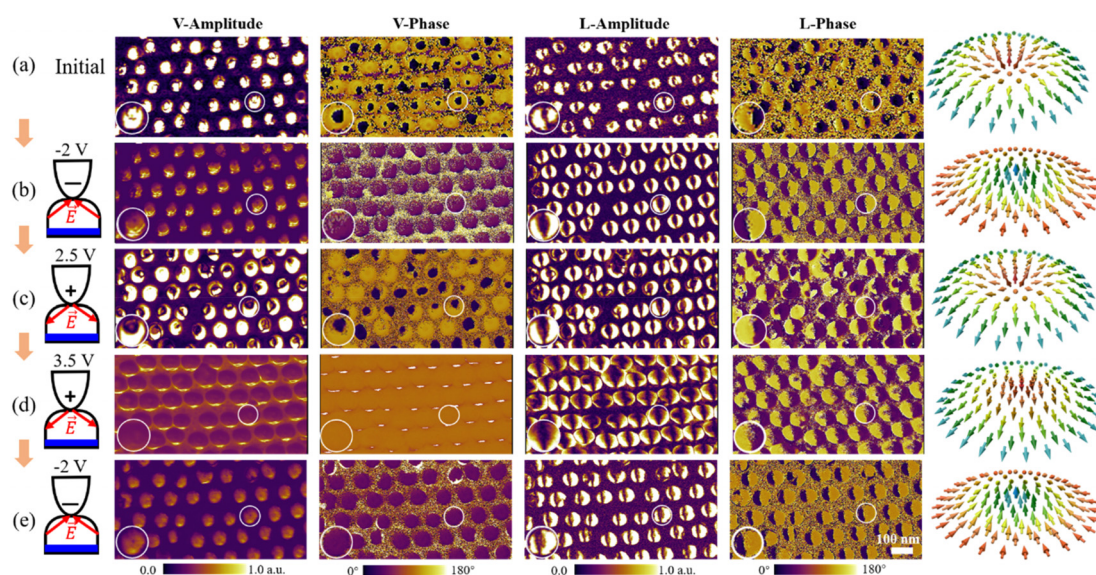


FIG. 4. (a) Vertical and lateral PFM amplitude and phase images and schematic three-dimensional polarization distribution of the nanodots marked with white circles. (b)–(e) The vector PFM images of the same region obtained after scanning the tip biased in sequence at -2.0 V (b), 2.5 V (c), 3.5 V (d), and -2.0 V (e).

ring-shaped conduction channels are distributed in the region of PTO nanodots (Fig. 5). The conduction channels are located on the hillsides of the nanodots, which exhibit large currents of 40 pA. We note that similar ring-shaped conduction channels were also observed in some BFO nanodots and nanoplates.^{34,41} Turning to the origins of the formation of ring-shaped conduction channels in our PTO nanodots, we mainly consider the following factors. First, it is worth mentioning that

the sample is prepared by converting the film into nanodots, and the surface of the PTO film undergoes etching. This process creates abundant surface defects, such as oxygen vacancies, which can reduce the Schottky barrier at the interface of Pt tip and PTO. Additionally, due to more severe etching on the hillsides of the nanodots compared to the peaks, a greater concentration of surface defects is distributed along the hillsides, making the Schottky barriers there much lower.

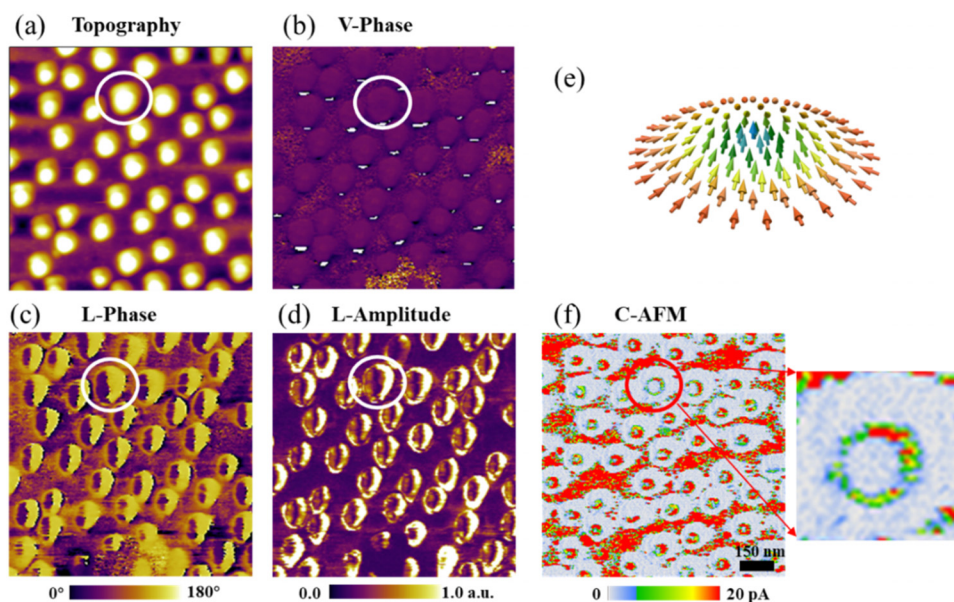


FIG. 5. (a)–(d) Topography (a), vertical PFM phase (b), lateral PFM phase (c), and amplitude (d) images of a PTO nanodots array, obtained after applied a write voltage of -2.0 V ($+2$ V bottom electrode bias in the CAFM mode). (e) Schematic three-dimensional polarization distribution of the polar nanodomain. (f) CAFM images of the same area shown in panels (a)–(d), obtained after applied a read voltage of -1.5 V ($+1.5$ V bottom electrode bias in CAFM mode).

This factor appears to play a significant role in the formation of ring-shaped conduction channels. Second, we propose that the center-convergent-type topological domain structures of the as-etched PTO nanodots could potentially temporarily stabilize the surface defects located at the hillsides. More specifically, the presence of negative polarization charges near the surfaces of hillsides may contribute to the stabilization of positively charged oxygen vacancies, preventing them from diffusing away or interacting with the atmosphere. Therefore, the Schottky barrier is lowered due to the presence of oxygen vacancies, which in turn contribute to the formation of ring-shaped conduction channels. In addition, there is a large polarization gradient in the center domains region of the nanodot that serve as traps for space charge to partially compensate the bound charges. Carriers associated with these space charges may be set free as long as the potential drop at hillsides of the nanodots bend the conduction band below the impurity levels, leading to an enhanced conductivity.

In summary, tunable center domains and skyrmion-like polar bubbles are observed in high-density PbTiO_3 nanodots on SrRuO_3 -buffered (001) STO substrate fabricated via the template-assisted tailoring of PTO thin films. Using vector PFM measurements, the polarization distribution of these nanodots is identified, which is similar to the spin configuration in small sized BFO nanodots (center domain states) and freestanding PTO layer (skyrmion-like polar bubbles). We are able to write and erase these topological domains by adjusting scanning bias applied on the conductive AFM tip. Moreover, ring-shaped conductive channels are observed around the center domain states. These findings suggest that reducing dimensions to the nanoscale is a promising strategy for manipulating and controlling topological defects, which in turn creates opportunities for extensive exploration of their emerging functionalities and application potentials in the field of nanoelectronics.

See the [supplementary material](#) for details on domain structures of the PTO film/nanodots, schematic flow chart illustrating the procedures of fabricating the PTO nanodots array, reciprocal space mapping of samples, and HAADF-STEM image and GPA ϵ_{xx} (in-plane) map of a part of a PTO nanodots.

The authors would like to thank the National Natural Science Foundation of China (Nos. U22A20117 and 92163210), the National Key Research and Development Programs of China (No. 2022YFB3807603), the Guangdong Basic and Applied Basic Research Foundation (Nos. 2023B1515130003, 2024A1515011608, and 2022A1515011727), the Guangdong Provincial Key Laboratory of Optical Information Materials and Technology (No. 2023B1212060065), and the Science and Technology Projects in Guangzhou (No. 202201000008). G.T. acknowledges support from the Hong Kong Scholar Program (No. XJ2022004).

AUTHOR DECLARATIONS

Conflict of Interest

The authors have no conflicts to disclose.

Author Contributions

Hongying Chen: Data curation (equal); Investigation (equal); Writing – original draft (supporting). **Zhiyu Liu:** Data curation (equal). **Guo Tian:** Conceptualization (lead); Funding acquisition (equal);

Project administration (equal); Writing – original draft (equal); Writing – review & editing (equal). **Gui Wang:** Investigation (equal). **Yihang Guo:** Investigation (equal). **Zongwen Duan:** Investigation (equal). **Di Wu:** Investigation (equal); Resources (equal); Supervision (equal). **Yu Deng:** Data curation (equal). **Guoyu Wang:** Investigation (equal); Resources (equal). **Zhipeng Hou:** Investigation (supporting). **Deyang Chen:** Investigation (supporting). **Zhen Fan:** Investigation (supporting). **Minghui Qin:** Funding acquisition (equal); Investigation (supporting). **Ji-Yan Dai:** Funding acquisition (equal); Writing – original draft (supporting). **Jun-Ming Liu:** Investigation (supporting). **Xingsen Gao:** Funding acquisition (equal); Investigation (equal); Project administration (equal); Writing – original draft (equal).

DATA AVAILABILITY

The data that support the findings of this study are available from the corresponding authors upon reasonable request.

REFERENCES

- A. K. Yadav, C. T. Nelson, S. L. Hsu, Z. Hong, J. D. Clarkson, C. M. Schlepütz, A. R. Damodaran, P. Shafer, E. Arenholz, L. R. Dedon, D. Chen, A. Vishwanath, A. M. Minor, L. Q. Chen, J. F. Scott, L. W. Martin, and R. Ramesh, “Observation of polar vortices in oxide superlattices,” *Nature* **530**, 198 (2016).
- C. Dai, V. A. Stoica, S. Das, Z. Hong, L. W. Martin, R. Ramesh, J. W. Freeland, H. Wen, V. Gopalan, and L. Q. Chen, “Tunable nanoscale evolution and topological phase transitions of a polar vortex supercrystal,” *Adv. Mater.* **34**, 2106401 (2022).
- W. Geng, X. Guo, Y. Zhu, Y. Tang, Y. Feng, M. Zou, Y. Wang, M. Han, J. Ma, B. Wu, W. Hu, and X. Ma, “Rhombohedral–orthorhombic ferroelectric morphotropic phase boundary associated with a polar vortex in BiFeO_3 films,” *ACS Nano* **12**, 11098 (2018).
- Y. L. Tang, Y. L. Zhu, and X. L. Ma, “Topological polar structures in ferroelectric oxide films,” *J. Appl. Phys.* **129**, 200904 (2021).
- E. Gradauskaitė, Q. N. Meier, N. Gray, M. F. Sarott, T. Scharsach, M. Campanini, T. Moran, A. Vogel, K. Del Cid-Ledezma, B. D. Huey, M. D. Russell, M. Fiebig, and M. Trassin, “Defeating depolarizing fields with artificial flux closure in ultrathin ferroelectrics,” *Nat. Mater.* **22**, 1492 (2023).
- S. W. Hu, X. F. Xiong, S. S. Luo, Y. Y. Liu, C. H. Lei, and K. Pan, “Regulation of flux-closure domain structures via oxygen vacancies and charged scanning probe microscopy,” *Appl. Phys. Lett.* **123**, 092901 (2023).
- Z. Li, Y. Wang, G. Tian, P. Li, L. Zhao, F. Zhang, J. Yao, H. Fan, X. Song, D. Chen, Z. Fan, M. Qin, M. Zeng, Z. Zhang, X. Lu, S. Hu, C. Lei, Q. Zhu, J. Li, X. Gao, and J.-M. Liu, “High-density array of ferroelectric nanodots with robust and reversibly switchable topological domain states,” *Sci. Adv.* **3**, e1700919 (2017).
- J. Ma, J. Ma, Q. Zhang, R. Peng, J. Wang, C. Liu, M. Wang, N. Li, M. Chen, X. Cheng, P. Gao, L. Gu, L. Q. Chen, P. Yu, J. Zhang, and C. W. Nan, “Controllable conductive readout in self-assembled, topologically confined ferroelectric domain walls,” *Nat. Nanotechnol.* **13**, 947 (2018).
- H. Chen, G. Tian, W. Yang, Z. Mo, L. Zhang, Y. Chen, C. Chen, Z. Hou, D. Chen, Z. Fan, X. Gao, and J.-M. Liu, “Complex center-type topological domain ferroelectric nanoislands rhombohedral $\text{Pb}(\text{Zr}_{0.7}\text{Ti}_{0.3})\text{O}_3$,” *J. Appl. Phys.* **128**, 224103 (2020).
- W. Yang, G. Tian, H. Fan, Y. Zhao, H. Chen, L. Zhang, Y. Wang, Z. Fan, Z. Hou, D. Chen, J. Gao, M. Zeng, X. Lu, M. Qin, X. Gao, and J.-M. Liu, “Nonvolatile ferroelectric-domain-wall memory embedded in a complex topological domain structure,” *Adv. Mater.* **34**, 2107711 (2022).
- X. Zhang, Y. Guo, G. Tian, Z. Song, C. Chen, W. Yang, Z. Hou, D. Chen, Z. Fan, G. Zhou, J.-M. Liu, and X. Gao, “Observation of center-type quad-domain structures in ordered BiFeO_3 nanoisland arrays fabricated via mask-assisted pulsed laser deposition,” *J. Appl. Phys.* **133**, 134103 (2023).
- S. Yan, X. Hu, X. Lu, S. Xiao, F. Huang, and X. Ying, “Large-scale optical manipulation of ferroelectric domains in PMN-PT crystals,” *Adv. Opt. Mater.* **10**, 2201092 (2022).

- ¹³S. Das, S. Y. L. Tang, Z. Hong, M. A. P. Goncalves, M. R. McCarter, C. Klewe, K. X. Nguyen, F. Gomez-Ortiz, P. Shafer, E. Arenholz, V. A. Stoica, S. L. Hsu, B. Wang, C. Ophus, J. F. Liu, C. T. Nelson, S. Saremi, B. Prasad, A. B. Mei, D. G. Schlom, J. Iniguez, P. Garcia-Fernandez, D. A. Muller, L. Q. Chen, J. Junquera, L. W. Martin, and R. Ramesh, "Observation of room-temperature polar skyrmions," *Nature* **568**, 368 (2019).
- ¹⁴L. Han, C. Addiego, S. Prokhorenko, M. Wang, H. Fu, Y. Nahas, X. Yan, S. Cai, T. Wei, Y. Fang, H. Liu, D. Ji, W. Guo, Z. Gu, Y. Yang, P. Wang, L. Bellaiche, Y. Chen, D. Wu, Y. Nie, and X. Pan, "High-density switchable skyrmion-like polar nanodomains integrated on silicon," *Nature* **603**, 63 (2022).
- ¹⁵S. Das, Z. Hong, V. A. Stoica, M. A. P. Goncalves, Y. T. Shao, E. Parsonnet, E. J. Marks, S. Saremi, M. R. McCarter, A. Reynoso, C. J. Long, A. M. Hagerstrom, D. Meyers, V. Ravi, B. Prasad, H. Zhou, Z. Zhang, H. Wen, F. Gomez-Ortiz, P. Garcia-Fernandez, J. Bokor, J. Iniguez, J. W. Freeland, N. D. Orloff, J. Junquera, L. Q. Chen, S. Salahuddin, D. A. Muller, L. W. Martin, and R. Ramesh, "Local negative permittivity and topological phase transition in polar skyrmions," *Nat. Mater.* **20**, 194 (2021).
- ¹⁶S. R. Bakaul, S. Prokhorenko, Q. Zhang, Y. Nahas, Y. Hu, A. Petford-Long, L. Bellaiche, and N. Valanoor, "Freestanding ferroelectric bubble domains," *Adv. Mater.* **33**, 2105432 (2021).
- ¹⁷J. Yin, H. Zong, H. Tao, X. Tao, H. Wu, Y. Zhang, L. D. Zhao, X. Ding, J. Sun, J. Zhu, J. Wu, and S. J. Pennycook, "Nanoscale bubble domains with polar topologies in bulk ferroelectrics," *Nat. Commun.* **12**, 3632 (2021).
- ¹⁸Q. Zhang, S. Prokhorenko, Y. Nahas, L. Xie, L. Bellaiche, A. Gruverman, and N. Valanoor, "Deterministic switching of ferroelectric bubble nanodomains," *Adv. Funct. Mater.* **29**, 1808573 (2019).
- ¹⁹Q. Zhang, L. Xie, G. Liu, S. Prokhorenko, Y. Nahas, X. Pan, L. Bellaiche, A. Gruverman, and N. Valanoor, "Nanoscale bubble domains and topological transitions in ultrathin ferroelectric films," *Adv. Mater.* **29**, 1702375 (2017).
- ²⁰X. Zhang, H. Chen, G. Tian, W. Yang, Z. Fan, Z. Hou, D. Chen, M. Zeng, M. Qin, J. Gao, X. Gao, and J.-M. Liu, "Creation and erasure of polar bubble domains in PbTiO₃ films by mechanical stress and light illuminations," *J. Materiomics* **9**, 626 (2023).
- ²¹Y. Nahas, S. Prokhorenko, Q. Zhang, V. Govinden, N. Valanoor, and L. Bellaiche, "Topology and control of self-assembled domain patterns in low-dimensional ferroelectrics," *Nat. Commun.* **11**, 5779 (2020).
- ²²Y. J. Wang, Y. P. Feng, Y. L. Zhu, Y. L. Tang, L. X. Yang, M. J. Zou, W. R. Geng, M. J. Han, X. W. Guo, B. Wu, and X. L. Ma, "Polar meron lattice in strained oxide ferroelectrics," *Nat. Mater.* **19**, 881 (2020).
- ²³D. Zheng, G. Tian, Y. Wang, W. Yang, L. Zhang, Z. Chen, Z. Fan, D. Chen, Z. Hou, X. Gao, Q. Li, and J.-M. Liu, "Controlled manipulation of conductive ferroelectric domain walls and nanoscale domains in BiFeO₃ thin films," *J. Materiomics* **8**, 274 (2022).
- ²⁴G. Tian, X. Yi, Z. Song, W. Yang, J. Xian, J. Jin, S. Ning, Z. Hou, D. Chen, Z. Fan, M. Qin, G. Zhou, J. Dai, X. Gao, and J.-M. Liu, "Templated growth strategy for highly ordered topological ferroelectric quad-domain textures," *Appl. Phys. Rev.* **10**, 021413 (2023).
- ²⁵J. J. P. Peters, G. Apachitei, R. Beanland, M. Alexe, and A. M. Sanchez, "Polarization curling and flux closures in multiferroic tunnel junctions," *Nat. Commun.* **7**, 13484 (2016).
- ²⁶J. M. Hu, L. Q. Chen, and C. W. Nan, "Multiferroic heterostructures integrating ferroelectric and magnetic materials," *Adv. Mater.* **28**, 15 (2016).
- ²⁷M. J. Han, Y. J. Wang, Y. L. Tang, Y.-L. Zhu, J. Y. Ma, W. R. Geng, M. J. Zou, Y. P. Feng, N. B. Zhang, and X. L. Ma, "Shape and surface charge modulation of topological domains in oxide multiferroics," *J. Phys. Chem. C* **123**, 2557 (2019).
- ²⁸A. Jiang and Y. Zhang, "Next-generation ferroelectric domain-wall memories: Principle and architecture," *npg Asia Mater.* **11**, 2 (2019).
- ²⁹G. Tian, W. D. Yang, X. S. Gao, and J.-M. Liu, "Emerging phenomena from exotic ferroelectric topological states," *APL Mater.* **9**, 020907 (2021).
- ³⁰G. Catalan, J. Seidel, R. Ramesh, and J. F. Scott, "Domain wall nanoelectronics," *Rev. Mod. Phys.* **84**, 119 (2012).
- ³¹A. Crassous, T. Sluka, A. K. Tagantsev, and N. Setter, "Polarization charge as a reconfigurable quasi-dopant in ferroelectric thin films," *Nat. Nanotechnol.* **10**, 614 (2015).
- ³²S. Dong, J.-M. Liu, S.-W. Cheong, and Z. Ren, "Multiferroic materials and magnetoelectric physics: Symmetry, entanglement, excitation, and topology," *Adv. Phys.* **64**, 519 (2015).
- ³³Y. Zheng and W. J. Chen, "Characteristics and controllability of vortices in ferromagnetics, ferroelectrics, and multiferroics," *Rep. Prog. Phys.* **80**, 086501 (2017).
- ³⁴K.-E. Kim, Y.-J. Kim, Y. Zhang, F. Xue, G.-Y. Kim, K. Song, S.-Y. Choi, J.-M. Liu, L.-Q. Chen, and C.-H. Yang, "Ferroelastically protected polarization switching pathways to control electrical conductivity in strain-graded ferroelectric nanoplates," *Phys. Rev. Mater.* **2**, 084412 (2018).
- ³⁵A. K. Yadav, K. X. Nguyen, Z. Hong, P. Garcia-Fernandez, P. Aguado-Puente, C. T. Nelson, S. Das, B. Prasad, D. Kwon, S. Cheema, A. I. Khan, C. Hu, J. Iniguez, J. Junquera, L. Q. Chen, D. A. Muller, R. Ramesh, and S. Salahuddin, "Spatially resolved steady-state negative capacitance," *Nature* **565**, 468 (2019).
- ³⁶N. Balke, B. Winchester, W. Ren, Y. H. Chu, A. N. Morozovska, E. A. Eliseev, M. Huijben, R. K. Vasudevan, P. Maksymovych, J. Britson, S. Jesse, I. Kornev, R. Ramesh, L. Bellaiche, L. Q. Chen, and S. V. Kalinin, "Enhanced electric conductivity at ferroelectric vortex cores in BiFeO₃," *Nat. Phys.* **8**, 81 (2012).
- ³⁷Z. Hong, A. R. Damodaran, F. Xue, S. L. Hsu, J. Britson, A. K. Yadav, C. T. Nelson, J. J. Wang, J. F. Scott, L. W. Martin, R. Ramesh, and L. Q. Chen, "Stability of polar vortex lattice in ferroelectric superlattices," *Nano Lett.* **17**, 2246 (2017).
- ³⁸G. Tian, D. Y. Chen, H. Fan, P. L. Li, Z. Fan, M. H. Qin, M. Zeng, J. Y. Dai, X. S. Gao, and J.-M. Liu, "Observation of exotic domain structures in ferroelectric nanodot arrays fabricated via a universal nanopatterning approach," *ACS Appl. Mater. Interfaces* **9**, 37219 (2017).
- ³⁹S. Kalinin, B. J. Rodriguez, S. Jesse, J. Shin, A. P. Baddorf, P. Gupta, H. Jain, D. B. Williams, and A. Gruverman, "Vector piezoresponse force microscopy," *Microsc. Microanal.* **12**, 206 (2006).
- ⁴⁰S. Cherifi-Hertel, H. Bulou, R. Hertel, G. Taupier, K. D. Dorkenoo, C. Andreas, J. Guyonnet, I. Gaponenko, K. Gallo, and P. Paruch, "Non-Ising and chiral ferroelectric domain walls revealed by nonlinear optical microscopy," *Nat Commun.* **8**, 15768 (2017).
- ⁴¹Z. W. Li, Z. Fan, and G. F. Zhou, "Nanoscale ring-shaped conduction channels with memristive behavior in BiFeO₃ nanodots," *Nanomaterials* **8**, 1031 (2018).
- ⁴²J. Hong, G. Catalan, D. N. Fang, E. Artacho, and J. F. Scott, "Topology of the polarization field in ferroelectric nanowires from first principles," *Phys. Rev. B* **81**, 172101 (2010).
- ⁴³I. Naumov and A. M. Bratkovsky, "Unusual polarization patterns in flat epitaxial ferroelectric nanoparticles," *Phys. Rev. Lett.* **101**, 107601 (2008).